Research Article Open Access

Alexander N. Shmakov, Svetlana V. Cherepanova, Dmitrii A. Zyuzin, Yulia E. Fedorova, Ivan A. Bobrikov, Anne-Cecile Roger, Andrzej Adamski, Vladislav A. Sadykov*

The crystal structure of compositionally homogeneous mixed ceria-zirconia oxides by high resolution X-ray and neutron diffraction methods

https://doi.org/10.1515/chem-2017-0044
received August 10, 2017; accepted November 22, 2017.

Abstract: The real/atomic structure of single phase homogeneous nanocrystalline $Ce_{0.5}Zr_{0.5}O_{2\pm\delta}$ oxides prepared by a modified Pechini route and Ni-loaded catalysts of methane dry reforming on their bases was studied by a combination of neutron diffraction, synchrotron X-ray diffraction, total X-ray scattering and X-ray absorption spectroscopy. The effects of sintering temperature and pretreatment in H_2 were elucidated. The structure of the mixed oxides corresponds to a tetragonal space group indicating a homogeneous distribution of Ce and Zr cations in the lattice. A pronounced disordering of the oxygen sublattice was revealed by neutron diffraction, supposedly due to incorporation of water into the structure when in contact with air promoted by the generation of anion vacancies in the lattice after reduction or calcination at high temperatures. However, such disordering has not resulted in any occupation of the oxygen interstitial positions in the bulk of the nanodomains.

Keywords: mixed ceria-zirconia oxides; neutron and X-ray diffraction studies; real/atomic structure; disordering

1 Introduction

Dry reforming of methane (DR) is now attracting a lot of attention because it converts cheap greenhouse gases into syngas with a H_2/CO ratio ~ 1, which is most suitable for synfuel production [1]. Mixed ceria-zirconia oxides promoted by inexpensive Ni are considered as promising catalysts of methane dry reforming due to their high activity, thermal and coking stability provided by a strong metal-support interaction along with a high mobility and reactivity of the support oxygen [2-7]. However, strong effects of the ceria-zirconia real/defect structure and spatial uniformity of Ce and Zr cations distribution in mixed oxides on the performance and coking resistivity of these catalysts were revealed as well [2-7]. In our work [8] a high performance and coking stability was demonstrated in the case of a catalyst comprised of Ni loaded on Ce-Zr-O prepared by the Pechini method using ethylene glycol as the solvent. For the optimization of such catalyst performance, its atomic structure controlling its oxygen mobility and reactivity is to be studied in detail, which is the aim of this work. Since structural features of these mixed oxides are very complex depending upon the spatial homogeneity of cation distribution in the oxide domains and oxygen stoichiometry, as well as the possible occupation of oxygen interstitial positions with formation of Frenkel defects [8-19], in this work neutron diffraction was used as the main technique since it is much more sensitive to the oxygen stoichiometry as compared with X-ray diffraction. Hence, detailed analysis of the oxygen stoichiometry effect on the real/defect structure of catalysts based on mixed ceria-zircinia oxides was the main purpose of this study.

***Corresponding author: Vladislav A. Sadykov:** Boreskov Institute of Catalysis, Novosibirsk, 630090, Russia; Novosibirsk State University, Novosibirsk, 630090, Russia, E-mail: sadykov@catalysis.ru
Alexander N. Shmakov, Svetlana V. Cherepanova, Dmitrii A. Zyuzin, Yulia E. Fedorova: Boreskov Institute of Catalysis, Novosibirsk, 630090, Russia
Alexander N. Shmakov, Svetlana V. Cherepanova: Novosibirsk State University, Novosibirsk, 630090, Russia
Ivan A. Bobrikov: Frank Laboratory of Neutron Physics, Joint Institute for Nuclear Research, Dubna, Moscow region, 141980, Russia
Anne-Cecile Roger: University of Strasbourg, Strasbourg, F-67087, France
Andrzej Adamski: Jagiellonian University, Krakow, Poland

2 Experimental

2.1 Catalyst Preparation

Dispersed Ce-Zr-O mixed oxides were prepared by a modified polymerized polyester precursor (Pechini) route [8]. At a constant stirring, metal nitrates were dissolved in an ethylene glycol mixture with citric acid followed by the dropwise addition of ethylenediamine. The mole ratios of citric acid (CA), ethylene glycol (EG) and ethylenediamine (ED) to the total metal ions in the solution were equal to 3.75:11.25:3.75:1. All reagents used for synthesis were of the "chemical pure grade". This viscous polymer was evaporated on a hot plate increasing the temperature to 100°C for 5 h followed by heating at 150°C for the next 5 h. A solid resin thus formed was burned under air at 600°C. The product thus obtained was ground with an agate pestle and mortar and calcined again under air at 600°C for 2 h. Ni (in amount of 10 wt.% Ni) was loaded by incipient wetness impregnation with a Ni nitrate solution followed by drying and calcination under air at 600°C. A part of the $Ce_{0.5}Zr_{0.5}O_{2\pm\delta}$ and $Ce_{0.5}Zr_{0.5}O_{2\pm\delta}$+10%Ni samples was calcined under air at 800°C and then a part of samples calcined at 800°C were reduced by mixture of 20 vol % H_2 in Ar with flow of 80 ml/min at 600°C for 3 h. There were therefore 6 different samples to investigate – two samples of $Ce_{0.5}Zr_{0.5}O_{2\pm\delta}$ calcined at 600°C and 800°C, two samples of $Ce_{0.5}Zr_{0.5}O_{2\pm\delta}$ loaded by Ni and calcined at 600°C and 800°C and two reduced samples of $Ce_{0.5}Zr_{0.5}O_{2\pm\delta}$ (800°C) and $Ce_{0.5}Zr_{0.5}O_{2\pm\delta}$+10%Ni (800°C).

2.2 Characterization of Catalysts

2.2.1 Neutron Diffraction

Neutron diffraction studies were carried out at the High Resolution Fourier Diffractometer (HRFD) installation in the Frank Laboratory of Neutron Physics of the Unified Institute for Nuclear Research in Dubna [20] using both high and low resolution modes. Diffraction data analysis was carried out using the FullProf software [21]. To minimize effects of statistical factors on the results of analysis, refinement of the structure of $Ce_{0.5}Zr_{0.5}O_{2\pm\delta}$ samples of a different genesis was carried out using low resolution diffraction patterns.

2.2.2 X-ray Diffraction and total X-ray scattering

Synchrotron X-ray Diffraction experiments of crystal structure parameters were performed at the "Precision Diffractometry" station in Siberian Synchrotron and the Terahertz Radiation Center of the Budker Institute of Nuclear Physics (Siberian Branch, Russian Academy of Sciences) [22]. The working photon energy (wavelength) was selected by a silicon (111) "channel-cut" monochromator with an energy resolution ~$3\cdot10^{-4}$. The photon flux on the sample is usually estimated as 10^8-10^9 phot/sec. The diffractometer operates in either high or low resolution mode with a Ge(111) crystal analyzer or a receiving slit in front of the scintillation detector. For $Ce_{0.5}Zr_{0.5}O_{2\pm\delta}$ oxide calcined at 600°C, the diffraction pattern in high resolution mode was recorded with λ=0.1127 nm in the 2Θ range of 10-90° and with a step size of $\Delta2\Theta$=0.05°. For refinement of its structure (space group $P4_2/nmc$:1) Rietveld analysis with a MAUD software was applied [23]. For $Ce_{0.5}Zr_{0.5}O_{2\pm\delta}$ 600°C, $Ce_{0.5}Zr_{0.5}O_{2\pm\delta}$ 800°C, 10%Ni-$Ce_{0.5}Zr_{0.5}O_{2\pm\delta}$ 600°C, 10%Ni-$Ce_{0.5}Zr_{0.5}O_{2\pm\delta}$ 800°C samples, diffraction data were collected in the low resolution mode with λ=0.07 nm radiation within the angular range 2Θ=3-140° and with a step size $\Delta2\Theta$=0.1°. The data were used for total X-ray scattering analysis to construct the radial distribution functions of the electron density (RDF).

2.2.3 X-ray absorption spectroscopy

The X-ray absorption spectra of the Ce L_{III}-edge (5.724 keV) as well as Zr and Ni K-edges (17.996 and 8.333 keV, respectively) were obtained at the "Structural Materials Science" beamline of Kurchatov Synchrotron Radiation Source at the National Research Center Kurchatov Institute [24]. The energy range of the beamline is 4.9-35 keV, with an energy resolution $\Delta E/E\sim2\cdot10^{-4}$. The radiation is emitted from the bending magnet with a photon flux on the sample of about $5\cdot10^7$ phot/(sec·mm^2) at a current of 100 mA. In particular experiments X-ray absorption data were collected in transmission mode and spectral analysis was carried out using Athena and Artemis software [25].

2.2.4 Thermal analysis

Thermogravimetric analysis was performed on a Netzsch STA 449C instrument. The sample temperature was linearly raised from 25°C to 900°C in a 100 ml/min He flow with a heating rate of 10°C/min.

Ethical approval: The conducted research is not related to either human or animals use.

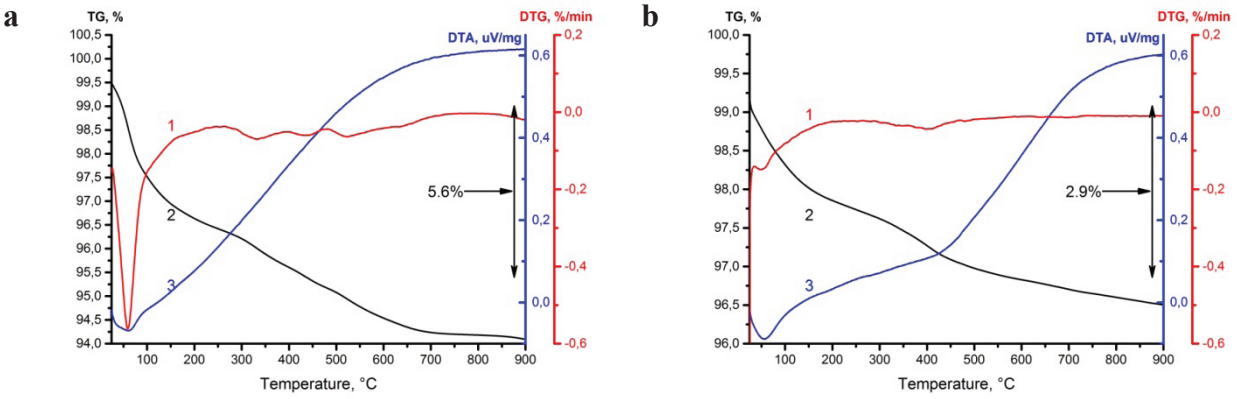

Figure 1: Typical thermal analysis data for $Ce_{0.5}Zr_{0.5}O_{2\pm\delta}$ oxides calcined at 600°C (a) and 800°C (b). 1 – DTG, 2 – TG, 3 – DTA.

3 Results and Discussion

3.1 Thermal analysis

Typical results of thermal analysis for $Ce_{0.5}Zr_{0.5}O_{2\pm\delta}$ samples are shown in Figure 1. For samples calcined at 600°C, a pronounced weight loss below 100°C is due to removal of adsorbed water while at higher temperatures bulk hydroxyls along with some amount of the lattice oxygen are removed [12]. For samples calcined at 800°C the weight loss is shifted to a higher temperature due to decreasing specific surface area and incorporation during cooling in air of some additional amount of hydroxyls into the lattice to fill anion vacancies formed due to removal of some lattice oxygen species at 800°C [12].

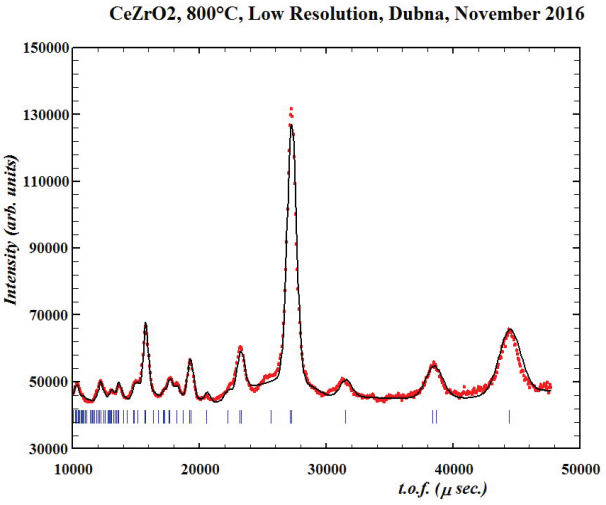

Figure 2: Experimental neutron diffraction pattern (points) and its fitting (solid line) for $Ce_{0.5}Zr_{0.5}O_{2\pm\delta}$ sample calcined at 800°C.

3.2 Neutron diffraction

Figure 2 presents experimental neutron diffraction pattern and its fitting for the $Ce_{0.5}Zr_{0.5}O_{2\pm\delta}$ sample calcined at 800°C. In all studied samples the structure of $Ce_{0.5}Zr_{0.5}O_{2\pm\delta}$ oxide corresponds to the tetragonal fluorite *t'* phase with $P4_2/nmc$ space group and c/a =1.01 [11,13,15]. Main structural parameters obtained by the data analysis are given in Table 1. In all cases uncertainty in estimation of these parameters is less than 10-11%.

The domain size estimated from refined profile parameters of the neutron diffraction pattern [21] of $Ce_{0.5}Zr_{0.5}O_{2\pm\delta}$ oxide tends to increase with the temperature of calcinations. The domain size of supported NiO is ~20 nm, while the size of Ni nanoparticles in the reduced sample is ~10 nm which is typical for mild reduction.

The oxygen stoichiometry values given in Table 1 demonstrate an apparent excess of oxygen in the lattice. This excess is largest for samples calcined at 800°C exceeding any possible estimated errors and not depending upon the applied procedure of the structure refinement. Since the synthesis procedure excludes the presence of any residual anions with a higher scattering ability as compared with oxygen anions, an alternative explanation is proposed. In the mixed oxide calcined at 600°C the oxygen content is close to the stoichiometry, while for samples calcined at 800°C a small fraction of the Ce cations can be reduced into +3 state with a loss of lattice oxygen [26]. Cooling of samples after calcinations under contact with air can result in water incorporation into some anion positions, thus leading to appearance of hydrogen in the lattice, for which neutron diffraction is sensitive as well. Since the orientation of the water molecule in these positions is flexible (rotation, etc), it can be considered as heavy-weighted oxygen, thus

Table 1: Refinement of the structural parameters of $Ce_{0.5}Zr_{0.5}O_{2\pm\delta}$ samples.

Sample	Phase composition	Volume fraction of phase, %	Unite cell parameters, nm	c/a_F^*	Oxygen stoichiometry	Domain size, nm
$Ce_{0.5}Zr_{0.5}O_2$, 600°C	$Ce_{0.5}Zr_{0.5}O_{2\pm\delta}$	100	*a*=0.3723(1) c=0.5302(3)	1.007	2.04(1)	6.1(5)
$Ce_{0.5}Zr_{0.5}O_2$, 800°C	$Ce_{0.5}Zr_{0.5}O_{2\pm\delta}$	100	*a*=0.3728(1) *c*=0.5312(4)	1.008	2.12(1)	7.0(5)
10%Ni(II) $Ce_{0.5}Zr_{0.5}O_2$, 600°C	$Ce_{0.5}Zr_{0.5}O_{2\pm\delta}$	70	*a*=0.3736(1) *c*=0.5289 (3)	1.001	2.03(1)	6.1(5)
	NiO	30	*a*=0.4178(1)			20.0(10)
10%Ni(II) $Ce_{0.5}Zr_{0.5}O_2$, 800°C	$Ce_{0.5}Zr_{0.5}O_{2\pm\delta}$	70	*a*=0.3732(1) *c*=0.5309(3)	1.006	2.17(1)	7.6(5)
	NiO	30	*a*=0.4180(1)			18.6(10)
$Ce_{0.5}Zr_{0.5}O_2$, 800°C, H_2	$Ce_{0.5}Zr_{0.5}O_{2\pm\delta}$	100	*a*=0.3727(1) *c*=0.5312(4)	1.008	1.90(1)	8.1(5)
10%Ni(II) $Ce_{0.5}Zr_{0.5}O_2$, 800°C, H_2	$Ce_{0.5}Zr_{0.5}O_{2\pm\delta}$	75	*a*=0.3742(1) *c*=0.5279(3)	0.998	1.98(1)	9.5(5)
	NiO	3	*a*=0.4180(4)			23.0(10)
	Ni^0	22	*a*=0.3525(1)			9.2(5)

*defined for the fluorite-like structure as c/a√2 [13]

explaining the apparent oxygen excess. Such an excess is more pronounced for Ni-loaded samples (Table 1), which can be due to the generation of additional oxygen vacancies due to incorporation of a fraction of Ni^{2+} cations in the mixed oxide lattice replacing some of the Ce^{4+}/Zr^{4+} cations. This is apparently reflected in the increase of the unit cell volume for Ni-loaded samples (Table 2). After reduction by H_2, oxygen stoichiometry is decreased as expected (Table 1), though some reoxidation of samples under contact with air even at room temperature could not be excluded as well. Indeed, the presence of some amount of NiO in the reduced sample (Table 1) agrees with such mild reoxidation.

The presence of the oxygen excess as bulk hydroxyls in nanocrystalline mixed ceria-zirconia oxides was earlier demonstrated by analysis of the total X-ray scattering data [27] as well as $^{18}O_2$ oxygen isotope heteroexchange data [28]. In the latter case, up to 3-4 monolayers of the excess oxygen were revealed by analysis of the gas phase balance while replacing ^{16}O in the oxide by ^{18}O from the labeled oxygen molecules [28].

To clarify the nature of the positions occupied by these water molecules/hydroxyls in the fluorite lattice, analysis was carried out for the model where additional oxygen atoms were placed into positions not occupied in the tetragonal unit cell. In this case, modeling revealed a sharp increase of isotropic temperature parameters up to senseless values, thus demonstrating the inadequacy of such schemes.

Table 2: Unit cell volume of $Ce_{0.5}Zr_{0.5}O_{2\pm\delta}$ oxides.

Sample	V, Å^3
$CeZrO_{2\pm\delta}$, 600°C	73.50
$CeZrO_{2\pm\delta}$, 800°C	73.81
Ni+$CeZrO_{2\pm\delta}$, 600°C	73.80
Ni+$CeZrO_{2\pm\delta}$, 800°C	73.93
$CeZrO_{2\pm\delta}$, 800°C +H_2	73.80
Ni+$CeZrO_{2\pm\delta}$, 800°C +H_2	73.92

Earlier, Mamontov et al [14,15] suggested a model of disordering of the oxygen sublattice in the cubic fluorite-like structure where a part of oxygen is shifted from basic O1 positions into interstitials O2: $CeO1_{2-c}O2_c$. Since in our case the structure is tetragonal, for modeling the coordinates of the interstitial position were recalculated from the cubic to tetragonal space group (Table 3).

Modeling revealed that attempts to apply such disordering in our case result in the increase of R-factors (the conventional factors of agreement between observed and calculated data) up to 19-20% even in the case of small occupations of O2 sites. This suggests that for samples of oxides studied in this work such a disordering does not take place.

Table 3: Transformation of atomic positions from cubic to tetragonal system.

	Cubic modification		Tetragonal modification	
Space group	**Fm3m**		**$P4_2/nmc$**	
Positions	Zr, Ce:	0.0, 0.0, 0.0	Zr, Ce:	0.0, 0.0, 0.0
	O1:	0.25, 0.25, 0.25	O1:	0.0, 0.5, 0.293
Centers of empty cubes		0.5, 0.5, 0.5		0.0, 0.0, 0.5
Additional O position (shifted from centers of empty cubes)	O2	0.354, 0.354, 0.5	O2:	0.0, 0.708, 0.5

3.3 X-ray diffraction and total X-ray scattering analysis

3.3.1 X-ray diffraction

Fitting of experimental data for the $Ce_{0.5}Zr_{0.5}O_{2\pm\delta}$ sample calcined at 600°C (Figure 3) in the $P4_2/nmc$:1 space group provides unit cell parameters a=0.37293(5) nm and c=0.5295(1) nm which are close to that estimated from neutron diffraction. Refinement of size and strain parameters gave a domain size of ~9.5-10.5 nm and microstrain close to 0.004. The oxygen position occupancy was found to be 1.06(3), which gives oxygen stoichiometry equal to 2.12(6) i.e. also close to the results of neutron diffraction analysis within estimated error (Table 1). The results of structure refinement of the $Ce_{0.5}Zr_{0.5}O_{2\pm\delta}$ sample calcined at 600°C are collected in Table 4.

In spite of poor statistics of the pattern and low sensitivity of X-ray diffraction to oxygen stoichiometry the results of $Ce_{0.5}Zr_{0.5}O_{2\pm\delta}$ structure analysis seem to be reasonable and goes in agreement with other implied methods.

3.3.2 Total X-ray scattering

Analysis of RDF curves (Figure 4) revealed that positions and intensities of peaks are better described for the model of the tetragonal structure with an R-factor ~ 10%. The main discrepancy between experimental and modeling curves is observed in the range of peaks corresponding to Me-O distances demonstrating a strong disordering of the oxygen sublattice in agreement with published data [27]. Moreover, one can see that the calculated peak which corresponds to a longer Me-Me distance is higher than the experimental peak, whereas neighboring maxima at 9.2 Å and 10.7 Å seem to be lower, that may be also caused by strong disordering at long distances.

Table 4: Results of Rietveld refinement of $Ce_{0.5}Zr_{0.5}O_{2\pm\delta}$ sample calcined at 600°C.

Structure parameters			
a, nm		0.37293(5)	
c, nm		0.5295(1)	
z_0		0.2247(1)	
	Ce	Zr	O
Occupancy	0.56	0.44	1.06
B factors	0.97	1.1	1.7
R_w, %		19.5%	

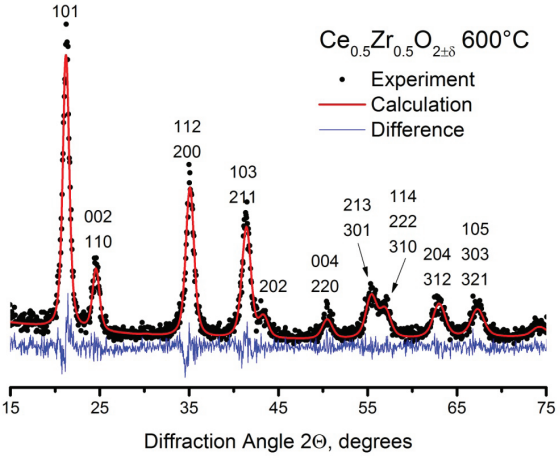

Figure 3: Experimental X-ray diffraction pattern (black points), its fitting (red solid line) and difference between experimental and calculated patterns (blue solid line) for $Ce_{0.5}Zr_{0.5}O_{2\pm\delta}$ sample calcined at 600°C.

3.4 X-ray absorption spectroscopy

X-ray absorption spectra of the samples recorded near CeL_{III}, ZrK and NiK absorption edges are shown in Figures 5, 6 and 7. For Ni the Fourier Transform (FT) of the absorption spectra is shown in Figure 8. Figures 5 and 6 demonstrate that CeL_{III} and ZrK spectra, despite of thermal or reducing treatments, are identical for all samples being close to that described earlier in our studies [27,29]. That means

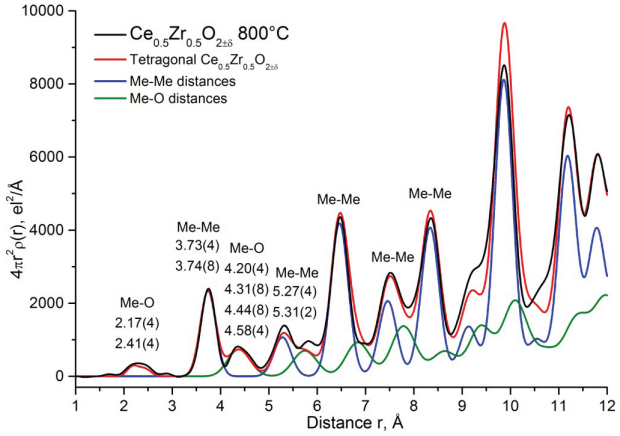

Figure 4: The pair distribution function (PDF) curve calculated from total X-ray scattering data for sample $Ce_{0.5}Zr_{0.5}O_{2\pm\delta}$ 800°C and model curves.

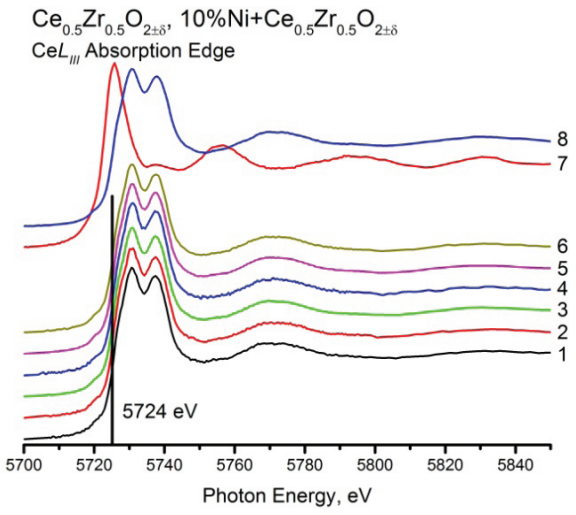

Figure 5: X-ray absorption spectra near CeL_{III} absorption edge: 1 – $Ce_{0.5}Zr_{0.5}O_{2\pm\delta}$ 600°C; 2 – $Ce_{0.5}Zr_{0.5}O_{2\pm\delta}$ 800°C; 3 – $Ce_{0.5}Zr_{0.5}O_{2\pm\delta}$ 800°C+H_2; 4 – Ni+ $Ce_{0.5}Zr_{0.5}O_{2\pm\delta}$ 600°C; 5 – Ni+$Ce_{0.5}Zr_{0.5}O_{2\pm\delta}$ 800°C; 6 – Ni+$Ce_{0.5}Zr_{0.5}O_{2\pm\delta}$ 800°C+H_2; 7 – Ce(III)AlO_3; 8 – Ce(IV)O_2.

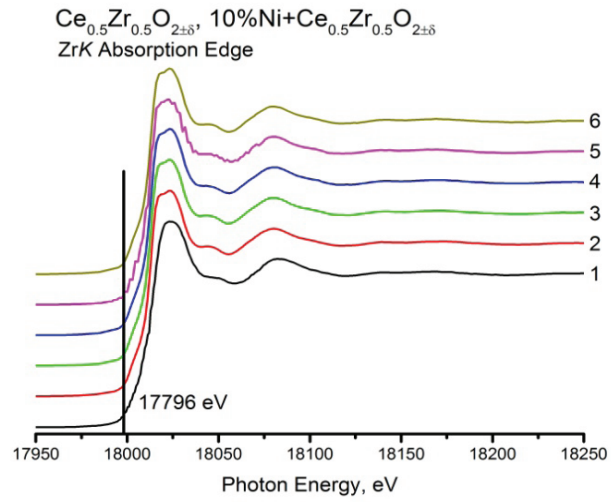

Figure 6: X-ray absorption spectra near Zr*K* absorption edge: 1 – $Ce_{0.5}Zr_{0.5}O_{2\pm\delta}$ 600°C; 2 – $Ce_{0.5}Zr_{0.5}O_{2\pm\delta}$ 800°C; 3 – $Ce_{0.5}Zr_{0.5}O_{2\pm\delta}$ 800°C+H_2; 4 – Ni+ $Ce_{0.5}Zr_{0.5}O_{2\pm\delta}$ 600°C; 5 – Ni+$Ce_{0.5}Zr_{0.5}O_{2\pm\delta}$ 800°C; 6 – Ni+$Ce_{0.5}Zr_{0.5}O_{2\pm\delta}$ 800°C+H_2.

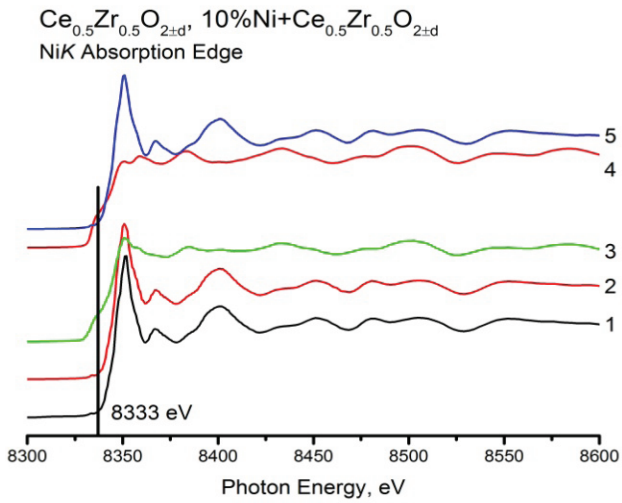

Figure 7: X-ray absorption spectra near Ni*K* absorption edge: 1 – Ni+ $Ce_{0.5}Zr_{0.5}O_{2\pm\delta}$ 600°C; 2 – Ni+$Ce_{0.5}Zr_{0.5}O_{2\pm\delta}$ 800°C; 3 – Ni+$Ce_{0.5}Zr_{0.5}O_{2\pm\delta}$ 800°C+H_2; 4 – Ni(0); 5 – Ni(II)O.

the local structure around Ce and Zr appears to be stable. The comparison of CeL_{III} spectra with that of standard samples Ce(IV)O_2 and Ce(III)AlO_3 leads to the conclusion that Ce remains in +4 state even in samples pretreated in hydrogen (Figure 6), which is explained by reoxidation of the mixed oxide support under contact with air even at room temperature.

Figures 7 and 8 indicate that for samples calcined under air at different temperatures the local structure of oxidized nickel is practically the same. The reduced sample contains a substantial amount of metallic nickel that one can see from the spectra and FT of NiO and metallic Ni standard samples.

The formation of the interaction phase due to incorporation of Ni into Ce-Zr mixed oxide lattice seems to be possible but hardly detectable because the amount of this phase would be very small. Both neutron diffraction and X-ray absorption spectroscopy demonstrate the presence of Ni oxide even in the reduced sample, so such a three-component system with a substantially different phase content is very difficult to analyze.

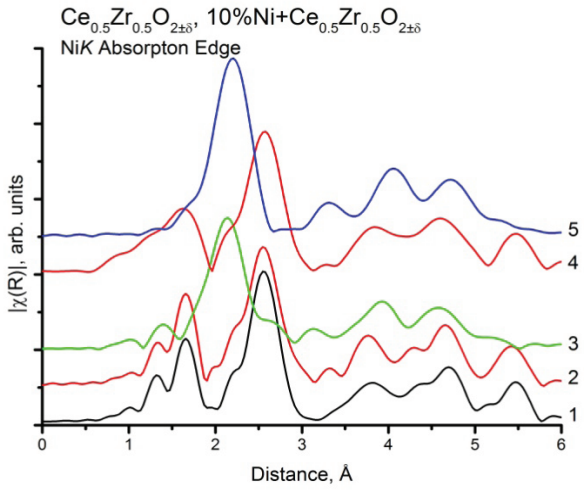

Figure 8: Fourier Transform of X-ray absorption spectra near Ni*K* absorption edge: 1 – Ni+ $Ce_{0.5}Zr_{0.5}O_{2\pm\delta}$ 600°C; 2 – Ni+$Ce_{0.5}Zr_{0.5}O_{2\pm\delta}$ 800°C; 3 – Ni+$Ce_{0.5}Zr_{0.5}O_{2\pm\delta}$ 800°C+H_2; 4 – Ni(0); 5 – Ni(II)O.

4 Conclusions

Studies of the real/atomic structure of single phase homogeneous nanocrystalline $Ce_{0.5}Zr_{0.5}O_{2\pm\delta}$ oxides prepared by a modified Pechini route by sophisticated diffraction methods revealed pronounced disordering of their oxygen sublattice due to formation of oxygen vacancies and consequent incorporation of water in their structure under contact with air. However, it has not resulted in any occupation of the oxygen interstitial positions in the bulk of the nanodomains. To confirm this statement, experiments on high temperature In Situ X-ray and neutron diffraction will be carried out and the results will be a matter of future report. The structure corresponds to a tetragonal space group indicating that there is a reasonably homogeneous distribution of Ce and Zr cations in the lattice. In general, the results obtained reasonably agree with those reported by Yashima et al. [30,31].

Acknowledgements: Support by NICE project of ERA Net Rus Plus Call and Russian Ministry of Education and Science under related contract №14.616.21.0036 (unique identifier of the contract RFMEFI61615X0036) is gratefully acknowledged. The part of the work related to the measurement of spectra has been done using the infrastructure of the Shared-Use Center "Siberian Synchrotron and Terahertz Radiation Center (SSTRC)" based on VEPP-3 of BINP SB RAS and supported by the project RFMEFI62117X0012 of the Ministry of Education and Science of The Russian Federation. The part of the work on neutron diffraction measurements has been done using the infrastructure of FLNP of JINR Dubna.

Conflict of interest: Authors state no conflict of interest.

References

[1] Verykios X. E., Catalytic dry reforming of natural gas for the production of chemicals and hydrogen, Int. J. Hydrogen Energy, 2003, 28, 1045–1063.

[2] Kambolis A., Matralis H., Trovarelli A., and Papadopoulou C., Ni/CeO_2-ZrO_2 catalysts for the dry reforming of methane, Appl. Catal. A-Gen., 2010, 377, 16–26.

[3] Montoya J. A., Romero-Pascual E., Gimon C., Del Angel P., and Monzón A., Methane reforming with CO_2 over Ni/ZrO_2–CeO_2 catalysts prepared by sol–gel, Catal. Today, 2000, 63, 71–85.

[4] Wolfbeisser A., Sophiphun O., Bernardi J., Wittayakun J., Föttinger K., and Rupprechter G., Methane dry reforming over ceria-zirconia supported Ni catalysts, Catal. Today, 2016, 277, 234–245.

[5] Chen J., Wu Q., Zhang J., and Zhang J., Effect of preparation methods on structure and performance of $Ni/Ce_{0.75}Zr_{0.25}O_2$ catalysts for CH_4-CO_2 reforming, Fuel, 2008, 87, 2901–2907.

[6] Roh H.-S., Potdar H. S., Jun K.-W., Kim J.-W., and Oh Y.-S., Carbon dioxide reforming of methane over Ni incorporated into Ce–ZrO_2 catalysts, Appl. Catal. A-Gen., 2004, 276, 231–239.

[7] Sukonket T., Khan A., Saha B., Ibrahim H., Tantayanon S., Kumar P., et al., Influence of the catalyst preparation method, surfactant amount, and steam on CO_2 reforming of CH_4 over $5Ni/Ce_{0.6}Zr_{0.4}O_2$ catalysts, Energy Fuels, 2011, 25, 864–877.

[8] Sadykov V.A., Simonov M.N., Mezentseva N.V., Pavlova S.N., Fedorova Y.E., Bobin A.S., et al., Ni-loaded nanocrystalline ceria-zirconia solid solutions prepared via modified Pechini route as stable to coking catalysts of CH_4 dry reforming, Open Chemistry , 2016, 14, 363–376.

[9] Acuña L.M., Fuentes R.O., Lamas D.G., Fábregas I.O., Walsöe de Reca N.E., Craievich A.F., High-temperature X-ray powder diffraction study of the tetragonal-cubic phase transition in nanocrystalline, compositionally homogeneous ZrO_2–CeO_2 solid solutions, Powder Diffraction, 2008, 23, 70–74.

[10] Alifanti M., Baps B., Blangenois N., Naud J., Grange P., Delmon B., Characterization of CeO_2 –ZrO_2 Mixed Oxides. Comparison of the Citrate and Sol–Gel Preparation Methods. Chemistry of Materials, 2003, 15, 395–403.

[11] Lamas D.G., Fuentes R.O., Fábregas I.O., Fernández de Rapp M.E., Lascalea G.E., Casanova J.R., et al., Synchrotron X-ray diffraction study of the tetragonal–cubic phase boundary of nanocrystalline ZrO_2 –CeO_2 synthesized by a gel-combustion process. Journal of Applied Crystallography, 2005, 38, 867–873.

[12] Larrondo S., Vidal M.A., Irigoyen B., Craievich A.F., Lamas D.G., Fábregas I.O., et al., Preparation and characterization of Ce/Zr mixed oxides and their use as catalysts for the direct oxidation of dry CH_4, Catalysis Today, 2005, 107-108, 53–59.

[13] Mamontov E., Brezny R., Koranne M., Egami T., Nanoscale Heterogeneities and Oxygen Storage Capacity of $Ce_{0.5}Zr_{0.5}O_2$, The Journal of Physical Chemistry B, 2003, 107, 13007–13014.

[14] Mamontov E., Egami T., Structural defects in a nano-scale powder of CeO_2 studied by pulsed neutron diffraction, Journal of Physics and Chemistry of Solids, 2000, 61, 1345–1356.
[15] Mamontov E., Egami T., Brezny R., Koranne M., Tyagi S., Lattice Defects and Oxygen Storage Capacity of Nanocrystalline Ceria and Ceria-Zirconia, The Journal of Physical Chemistry B, 2000, 104, 11110–11116.
[16] Meriani S., Features of the Caeria-Zirconia systems, Materials Science and Engineering: A, 1989, 109, 121–130.
[17] Meriani S., A new single-phase tetragonal CeO_2-ZrO_2 solid solution, Materials Science and Engineering, 1985, 71, 369–370.
[18] Meriani S., Spinolo G., Powder Data for Metastable $Zr_xCe_{1-x}O_2$ (x = 0.84 to 0.40) Solid Solutions with Tetragonal Symmetry, Powder Diffraction, 1987, 2, 255–256.
[19] Monte R.D., Kašpar J., Nanostructured CeO_2 –ZrO_2 mixed oxides, J. Mater. Chem., 2005, 15, 633–648.
[20] Balagurov A.M., Bobrikov I.A., Bokuchava G.D., Zhuravlev V.V., Simkin V.G., Correlation Fourier diffractometry: 20 Years of experience at the IBR-2 reactor, Physics of Particles and Nuclei, 2015, 46, 249–276.
[21] Rodriguez-Carvajal, J., Recent advances in magnetic structure determination by neutron powder diffraction, Physica B, 1993, 192, 55-65.
[22] Shmakov A.N., Tolochko B.P., Dementiev E.N., Sheromov M.A., The modified experimental X-ray powder diffraction station on the SR beamline no. 2 of VEPP-3 storage ring, Journal of Structural Chemistry, 2016, 57, 1321–1326.
[23] Lutterotti L., Total pattern fitting for the combined size–strain–stress–texture determination in thin film diffraction, Nuclear Instruments and Methods in Physics Research Section B: Beam Interactions with Materials and Atoms, 2010, 268, 334–340.
[24] Chernyshov A.A., Veligzhanin A.A., Zubavichus Y.V., Structural Materials Science end-station at the Kurchatov Synchrotron Radiation Source: Recent instrumentation upgrades and experimental results, Nuclear Instruments and Methods in Physics Research Section A: Accelerators, Spectrometers, Detectors and Associated Equipment, 2009, 603, 95–98.
[25] Ravel, B., Newville, M., *ATHENA*, *ARTEMIS*, *HEPHAESTUS:* data analysis for X-ray absorption spectroscopy using *IFEFFIT*, Journal of Synchrotron Radiation, 2005, 12, 537–541.
[26] Sadykov V.A., Frolova-Borchert Yu.V., Mezentseva N.V., Alikina G.M., Lukashevich A.I., Paukshtis E.A., et al., Nanocrystalline catalysts based on CeO_2-ZrO_2 doped by praseodymium or gadolinium: synthesis and properties, Mater. Res. Soc. Symp. Proc., 2006, 900E, O10.04-1-6
[27] Sadykov V.A., Mezentseva N., Alikina G., Lukashevich A., Muzykantov V., Kuznetsova T., et al., Nanocrystalline Doped Ceria-Zirconia Fluorite-Like Solid Solutions Promoted by Pt: Structure, Surface Properties and Catalytic Performance in Syngas Generation, Mater. Res. Soc. Symp. Proc., 2006, 988, QQ06-04-1-6.
[28] Sadovskaya E.M., Ivanova Y.A., Pinaeva L.G., Grasso G., Kuznetsova T.G., van Veen A., et al., Kinetics of Oxygen Exchange over CeO_2–ZrO_2 Fluorite-Based Catalysts, The Journal of Physical Chemistry A, 2007, 111, 4498–4505.
[29] Sadykov V., Mezentseva N., Alikina G., Lukashevich A., Muzykantov V., Bunina R., et al., Doped Nanocrystalline Pt-Promoted Ceria-Zirconia as Anode Catalysts for IT SOFC: Synthesis and Properties, Mater. Res. Soc. Symp. Proc., 2007, 1023, JJ02-07-1-6.
[30] Yashima M., Sasaki S., Yamaguchi Y., Kakihana M., Yoshimura M., Mori T., Internal distortion in ZrO_2–CeO_2 solid solutions: Neutron and high-resolution synchrotron x-ray diffraction study, Applied Physics Letters, 1998, 72, 182–184.
[31] Yashima M., Wakita T., Atomic displacement parameters and structural disorder of oxygen ions in the $Ce_xZr_{1-x}O_2$ solid solutions ($0.12 \leq x \leq 1.0$): Possible factors of high catalytic activity of ceria-zirconia catalysts, Applied Physics Letters, 2009, 94, 171902-1-3.